Dimethylformamide-mediated polymer microstructure dictates the extensional rheology of aqueous PNIPAM solutions

Diana Y. Zhang, Alec J. Schwendinger, and Michelle A. Calabrese*

Department of Chemical Engineering and Materials Science, University of Minnesota, Minneapolis, MN 55455

E-mail: mcalab@umn.edu

TOC Graphic

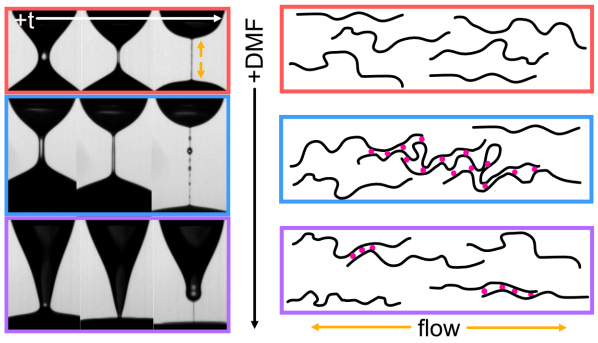

Abstract

Polymer solution processability in extensional-flow dominated operations is strongly influenced by polymer conformation and solution phase behavior. Cosolvent addition can be used to tailor polymer conformation and solution phase behavior to yield formulations that are amenable to processes such as spraying and atomization, coating, and fiber spinning. The addition of N,N-dimethylformamide (DMF) to aqueous poly(N-isopropylacrylamide) (PNIPAM) solutions induces unique phase behavior and

microstructure formation, yet the effects on solution processability have remained unexplored. In this work, the effect of DMF cosolvent content on the rheology (both shear and extensional) and microstructure of PNIPAM solutions is investigated. While all examined PNIPAM solutions exhibit nearly Newtonian steady shear behavior regardless of DMF content, the same solutions exhibit varying degrees of extensibility. Surprisingly, the extensional relaxation time (λ_E) increases by more than twenty-fold with increasing DMF content in the water-rich regime. In the DMF-rich regime, however, solution extensibility dramatically decreases. Interestingly, this unique variation in extensional flow behavior does not scale as expected based on changes in the measured intrinsic viscosity and radius of gyration. Instead, a mechanism is proposed that relates the extensional flow behavior to the solution microstructure, which is found to vary with DMF content in light scattering measurements. In the water-rich regime, DMF molecules are proposed to bridge PNIPAM chains via hydrogen bonding and hydrophobic interactions, resulting in physically crosslinked aggregates. In extensional flows, these aggregates behave like a polymer with higher apparent molecular weight, increasing λ_E. In the DMF-rich regime, non-bridging DMF molecules increasingly solvate individual PNIPAM chains; consequently, more individual chains are stretched in extensional flows, leading to a reduction in λ_E. These findings demonstrate that interactions between components in these ternary systems have unexpected but significant implications in solution extensional flow behavior. Additionally, in the case of PNIPAM/DMF/water, the processability of polymer-containing formulations can be modulated for spraying or for fiber spinning applications just by varying cosolvent (DMF) content.

Introduction

Stimuli-responsive polymers can reversibly change polymer conformation and properties in response to external stimuli and are therefore of great interest for numerous applications. Thermoresponsive polymers in particular respond to changes in temperature, and this feature has been leveraged for a variety of applications including smart coatings,[1,2] separations,[3–5] and water remediation.[6,7] One of the most well-studied thermoresponsive polymers is poly(N-isopropylacrylamide) (PNIPAM). PNIPAM is known to undergo a significant conformational change upon reaching the lower critical solution temperature (LCST) at ∼32 °C in purely aqueous solution.[8] Below the LCST, the polymer chains are solvated and exist as random coils in solution. Above the LCST, the coils collapse and aggregate into globules as the translational entropy of the released solvent molecules dominates the enthalpy of PNIPAM-water hydrogen bonding.[8,9]

The realization of PNIPAM-based applications often involves extensional-flow dominated solution processing; for example, coatings,[10] membranes,[11,12] and electrodes[4] are often manufactured at scale using coating, spraying and atomization, and fiber spinning processes.[13–16] While prior studies have demonstrated the importance of tuning PNIPAM solution phase behavior and polymer conformation for various applications,[1,2,17] these same features also have implications in the flow behavior of PNIPAM solutions in extensional-flow dominated processes. For example, polymer conformation and self-assembly dramatically impact solution extensibility: solutions of spherical micelles exhibit Newtonian extensional flow behavior while, in contrast, solutions of high molecular weight polymers and wormlike micelles exhibit viscoelastic extensional flow behavior and Trouton ratios exceeding $O(10^2)$.[18,19] Additionally,

as temperature is often optimized during solution processing operations – including to modulate droplet size distribution[20] or fiber morphology[21] – it is also desirable to tune the phase transition temperature and polymer conformation of PNIPAM-based polymer solutions to ensure formulations are processable at specific conditions.

The LCST of PNIPAM in purely aqueous solution is, however, largely independent of polymer molecular weight and concentration,[22,23] which limits the ability to tune phase transition temperature and polymer conformation. PNIPAM can be copolymerized with hydrophilic or hydrophobic monomers to tune the phase transition and underlying polymer microstructure,[24–26] but this strategy requires changes in the polymer chemistry. Additionally, additives such as surfactants have been leveraged to tune the LCST of aqueous PNIPAM;[27,28] however, the presence of surfactant can greatly affect PNIPAM surface properties and thus prove detrimental to coating uniformity.[29]

Alternatively, cosolvent addition can be leveraged to tune phase transition temperature and polymer conformation in aqueous PNIPAM and PNIPAM-based polymer solutions without changing polymer chemistry.[30–33] Cosolvent addition is already often leveraged to control fiber spinning morphology towards membranes and electrodes with certain microstructures or properties.[16,34,35] Thus, cosolvent addition can serve as a simple, synergistic strategy to tune the processability of PNIPAM-based polymer solutions. However, adding a cosolvent to aqueous PNIPAM solutions often gives rise to complex phase behavior. In fact, the addition of a second good solvent to PNIPAM/water solutions can cause PNIPAM to become immiscible at certain solvent compositions and temperatures – a phenomenon termed cononsolvency.[30,36] Cononsolvency has been attributed to changes in attractive interactions between

bulk solvent and cosolvent as well as preferential polymer-solvent and polymer-cosolvent interactions.[36]

While the exact phase behavior of PNIPAM in cosolvent/water mixtures depends on solvent identity, cosolvent addition generally affects the phase behavior in two ways. In the first case, the solution exhibits LCST behavior across a range of cosolvent concentrations; in water-rich solutions, the LCST decreases with cosolvent content. The LCST exhibits a minimum at some composition, then increases with cosolvent content in the cosolvent-rich regime.[30] In the second case, the solution exhibits an LCST that decreases as a function of cosolvent content in the water-rich regime and an upper critical solution temperature (UCST) that decreases with cosolvent content in the cosolvent-rich regime (e.g. dimethylsulfoxide, N,N-dimethylformamide, ethanol).[30] At intermediate cosolvent content, the phase diagram can exhibit a two-phase window wherein PNIPAM is immiscible across all temperatures.[30] With the diversity of solvents that impart cononsolvency and the range of possible phase behavior, the cononsolvency phenomenon can be leveraged not only to modulate the transition temperature but also to modulate polymer conformation[37] and thus processability at fixed temperature.

While PNIPAM/N,N-dimethylformamide (DMF)/water systems remain relatively understudied compared to PNIPAM/alcohol/water systems, several studies[33,38] have shown that incorporating DMF into aqueous PNIPAM-based systems leads to interesting properties and behaviors that are hypothesized to arise from changes in polymer-solvent, polymer-cosolvent, and solvent-cosolvent hydrogen bonding interactions. Zhu and Chen[38] characterized the cononsolvency behavior of aqueous, chemically crosslinked PNIPAM microgel solutions in

the presence of varying amounts of DMF. The authors showed that PNIPAM microgels below the LCST undergo conformational collapse followed by re-swelling at intermediate DMF contents, reflective of cononsolvency behavior. Supported by mean field calculations, the authors attributed this reentrant transition behavior to preferential DMF adsorption and bridging of PNIPAM segments. Recently, Linn et al.[33] showed that incorporating 3-(trimethoxysilyl)propyl methacrylate (TMA) comonomer into PNIPAM-based polymers leads to a decrease in the cloud point temperatures, T_{CP}, relative to PNIPAM homopolymer, and the magnitude of change increases with DMF content. The authors posited that the decrease in T_{CP} results from a combination of changes in polymer-solvent and solvent-cosolvent interactions; namely, the number of available hydrogen bonding donor sites decrease as TMA incorporation increases, and DMF disrupts the tetrahedral structure of water above $\sim$13.5% mol.[39] These few studies on PNIPAM-DMF-water systems report unique effects of DMF addition on the microstructure and phase behavior of PNIPAM-containing polymers; however, no studies have yet explored how the DMF-induced microstructure and phase behavior affect solution processability.

In this work, the extensional flow behavior of aqueous PNIPAM solutions with varying DMF content is characterized to assess the effects of DMF on PNIPAM solution processability. Dripping-onto-substrate (DoS) extensional rheometry measurements of PNIPAM solutions below the LCST show that the solution extensibility varies dramatically with DMF content in both one-phase regions. In contrast, steady shear rheology measurements reveal largely Newtonian behavior. Meanwhile, the calculated intrinsic viscosities indicate that underlying solution microstructure unexpectedly varies with DMF content. Dynamic and

static light scattering measurements provide further insight into the effects of DMF on PNIPAM solution microstructure, informing a proposed mechanism that links DMF-induced microstructure to solution extensional flow behavior. The results of this study demonstrate that cosolvent content affects the interactions among polymer, solvent, and cosolvent molecules and consequently solution microstructure, which has significant implications in PNIPAM-based solution processability. By simply varying cosolvent content, these interactions can be leveraged to modulate processability when designing formulations for extensional-flow dominated processes such as spraying, coating, and fiber spinning.

Materials and methods

Materials and solution preparation

Poly(N-isopropylacrylamide) (PNIPAM) (weight-average molecular weight $M_w = 9.49 \cdot 10^5$ g/mol, Đ= 3.02, SI.1) was used as received from Scientific Polymer Products, Inc. PNIPAM solutions were prepared by dissolving polymer powder in distilled water and N,N-dimethylformamide (used as received, Certified ACS, Fisher Scientific). Solutions were then placed on an orbital shaker at 4 °C for at least 12 hours prior to cloud point, rheology, and light scattering measurements.

Cloud point testing

Cloud point testing was used to determine the optical transition temperature of PNIPAM solutions as a function of DMF content. Cloud point measurements were obtained using a custom-built turbidimetry instrument equipped with a 405 nm violet laser (5 mW) and 637 nm red laser.[40] A set protocol was used to heat and cool each solution to minimize variability

between samples: equilibrate at 20 °C for 5 min; heat from 20 °C to 45 °C at 0.2 °C/min; equilibrate at 45 °C for 5 min; cool from 45 °C to 20 °C at a rate of 0.2 °C/min. While the cloud point temperature (T_{CP}) can be quantified using a number of approaches, here T_{CP} was determined from the inflection point of the heating curve rather than the transition onset (Figure S2), as recommended by Osváth and Iván [41]. This method of determining T_{CP} also corresponds better with the temperature of the peak in differential scanning calorimetry measurements of the phase separation enthalpy. [40,42]

Shear rheology

The shear rheology of PNIPAM solutions was measured at 21 °C using an Anton Paar MCR 302 stress-controlled rheometer equipped with a 50 mm cone and plate geometry. A Peltier hood was used during all measurements to minimize sample evaporation. Prior to each measurement, a pre-shear protocol was used. Here, a steady shear rate, $\dot{\gamma}$, of 10 s^{-1} was applied for 2 s, followed by an oscillatory shear with a strain amplitude, γ_0, of 0.1 % at an angular frequency, ω, of 1 rad/s for 2 s. Steady shear measurements were then taken by measuring the shear stress τ (and thus viscosity η via $\eta = \tau/\dot{\gamma}$) while ramping up in shear rate over the range $\dot{\gamma}$ = 1 s^{-1} to 1000 s^{-1}, followed by a ramp-down protocol over the same range. All solutions in this study were Newtonian or weakly shear thinning, so zero-shear viscosity values (η_0) were estimated by averaging over a range of shear rates in the Newtonian regime where sufficient signal was obtained, typically between $\dot{\gamma}$ = 10 and 100 s^{-1}.

Static and dynamic light scattering

Samples were prepared by dissolving PNIPAM at a concentration 0.1% wt (below the overlap concentration c^*, Table S3) in distilled water and DMF. Solutions were then filtered through 0.45 μm wwPTFE filters directly into measurement tubes. Light scattering measurements were taken using a Brookhaven BI-200SM instrument with a 637 nm laser at 21 °C.

Dynamic light scattering (DLS) measurements were used to determine the hydrodynamic radius R_h of PNIPAM coils as a function of DMF content. DLS scans were taken for 5 minutes each at measurement angles θ = 60, 75, 90, 105, and 120°. The data were first analyzed using the REPES Laplace inversion routine to determine the number of populations (SI.7.1).[43] Then, R_h was determined by fitting autocorrelation curves to the appropriate second cumulant or double exponential model to extract diffusion coefficients, then using the Stokes-Einstein relation to calculate R_h (SI.7.1). 95% confidence intervals of R_h values were calculated from propagated standard errors of the slopes in plots of decay rate Γ vs. the square of the scattering vector magnitude q^2 (Figure S13).

Static light scattering (SLS) was used to determine the radius of gyration R_g of PNIPAM coils as a function of DMF content. SLS scans were taken for angles θ = 30° to 135° (1 second each, 5 repeats per angle). The total counts were kept around 100,000 for each measurement by adjusting the aperture between 1 mm and 3 mm and using laser attenuation filters. Guinier plots for each solvent composition were constructed to determine R_g values (SI.8.1). For solutions in which at least three multi-angle datasets were obtained ($\geq$ 10% mol DMF), average R_g values and 95% confidence intervals were determined across multiple trials. For solutions in which only one multi-angle dataset was obtained (0, 5% mol DMF),

95% confidence intervals were calculated from propagated standard errors of the slope in Guinier plots (Figure S15).

Dripping-onto-substrate extensional rheometry

The extensional rheology of PNIPAM solutions was measured using dripping-onto-substrate (DoS) extensional rheometry, a technique pioneered by Dinic et al.[44] The instrumentation and methodology for measurements at ambient conditions (T = 21 °C) were described in detail previously.[18,45] Briefly, the DoS instrument consists of a dispensing system, a light source, and an imaging system. The test fluid is extruded through an 18 gauge (OD = 1.27 mm) blunt tip nozzle with a flow rate of 200 μL/hr to form a pendant drop. A glass substrate is then slowly raised using a micrometer screw to contact the droplet, forming a liquid bridge that then undergoes capillary-driven thinning. The spatiotemporal evolution of the liquid bridge is captured using a Chronos 1.4 high-speed camera, with frame rates ranging from 5,000 to 11,806 fps to maximize resolution depending on the duration of thinning. Frames from high-speed videos were then processed using an in-house MATLAB edge detection code to yield radius evolution curves. The extensional relaxation time, λ_E, for each trial was determined from fits to the elastocapillary regime prior to the onset of the beads on a string elastic instability (SI.3.3). At least three trials were taken for each solution composition, and the average and 95% confidence intervals across multiple trials are reported for the extensional relaxation time.

Results

Phase behavior of PNIPAM in DMF/water mixtures

The temperature vs. DMF content phase diagram for PNIPAM solutions (c = 0.5% wt) exhibits lower critical solution temperature (LCST) transitions from 0% to 15% mol DMF, in agreement with previous studies[30,33,46] (Figure 1). In this water-rich regime, the cloud point temperature, T_{CP}, varies non-monotonically with DMF content, exhibiting a maximum near 5% mol DMF. At low DMF content (<5% mol), T_{CP} increases with DMF content as preferential interactions between DMF and PNIPAM stabilize the hydrated polymer conformation.[30,33,46] As DMF content increases further, the cloud point temperature decreases as DMF molecules increasingly interact with water molecules and impact the hydration of PNIPAM chains. DMF is generally considered a chaotrope[38,47] – or a structure breaker – as DMF molecules break up the tetrahedral structure of water molecules above 13.5% mol DMF.[39]

In DMF-rich solutions, upper critical solution temperature (UCST) rather than LCST behavior is observed, and the cloud point temperature decreases with DMF content[30] (Figure 1). The transition to UCST behavior has been attributed to the shift from hydrogen bonding interactions at lower DMF contents to dominant dipole-dipole interactions at high DMF contents.[30] The presence of an intermediate two-phase region in which PNIPAM is immiscible is characteristic of cononsolvency behavior, which results from changing PNIPAM-DMF-water interactions.[36]

In the one-phase regions, PNIPAM chains are solvated, and the solution is optically clear; in the two-phase region, PNIPAM chains are collapsed and aggregated, resulting in a

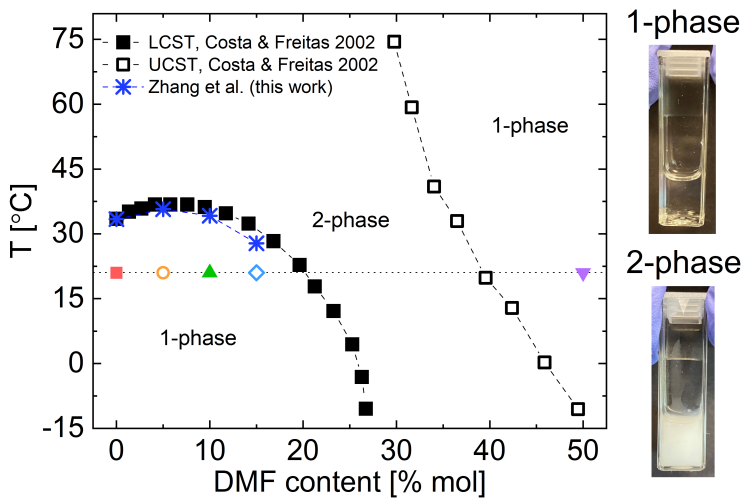

Figure 1: Phase diagram indicating LCST and UCST transitions of PNIPAM in DMF/water mixtures with representative images of one-phase (optically clear) and two-phase (turbid) solutions. The cloud point temperatures, T_{CP}, in this study for 0.5% wt PNIPAM solutions agree well with those previously reported by Costa and Freitas[30] (co-plotted) and Linn et al.[33] Symbols along black horizontal line at T = 21 °C indicate the temperature and compositions at which all rheological and light scattering measurements are conducted.

turbid suspension (Figure 1 images). Accordingly, subsequent rheological and light scattering measurements are conducted only in the one-phase regions of the phase diagram in Figure 1, indicated by the symbols along the horizontal line at T = 21 °C. Measurements sweep DMF concentrations from 0% to 15% mol in the LCST region and DMF concentrations of 50% and 100% mol in the UCST region. Cloud point temperature (CPT) measurements were not conducted for 50% mol DMF solutions as the corresponding cloud point temperature (T_{CP} $\sim$ -10 °C[30]) is beyond the limitations of the instrument. Measurements were not conducted in the intermediate two-phase region due to PNIPAM collapse, aggregation, and phase separation.[38,48,49]

Effect of DMF content on solution extensional flow behavior

Extensional rheology of water-rich solutions

Dripping-onto-substrate (DoS) extensional rheometry measurements of PNIPAM solutions reveal dramatic changes in extensional flow behavior as DMF content increases in the water-rich, one-phase regime. DoS measurements capture the minimum radius of a liquid bridge that self-thins in time. All DoS radius evolution curves of PNIPAM solutions at a fixed polymer concentration $c = 0.5\%$ wt with DMF content ranging from 0% to 15% mol exhibit two distinct thinning regimes (Figures 2a, S3). The first thinning regime can be described by a power law fit with an exponent $n = 2/3$ in accordance with the inertiocapillary (IC) thinning model. This model describes the self-similar thinning behavior of inviscid, inelastic fluids:[50–52]

$$\frac{R_{min}}{R_0} = \alpha \left(\frac{t_b - t}{t_R} \right)^{2/3} \tag{1}$$

Here, α is a prefactor, R_{min} is the minimum fluid filament radius, R_0 is the initial filament radius, and t_b is the pinch-off or break up time for the liquid bridge. The characteristic Rayleigh timescale is $t_R = \sqrt{\rho R_0^3/\sigma}$ for a fluid with density ρ and surface tension σ. Representative IC fits are shown in Figure S4. The IC thinning behavior observed at early times is expected as the PNIPAM solutions with 0% to 15% mol DMF are relatively dilute and low-viscosity. Here, the Ohnesorge number $Oh = \eta/\sqrt{\sigma \rho R_0}$, which compares viscous forces – represented by shear viscosity η – to surface tension and inertial forces acting on the fluid, for each solution is $Oh \ll 1$. Such values of Oh indicating that thinning behavior is dominated

by surface tension and inertial forces (Table S1).

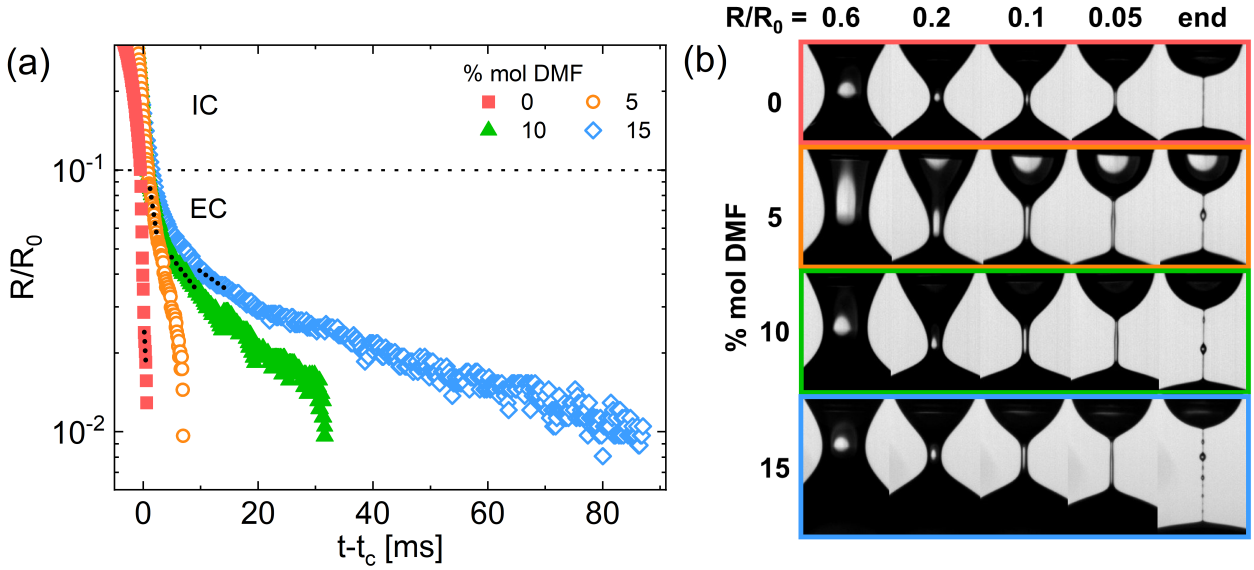

Figure 2: Extensional flow behavior of 0.5% wt PNIPAM in 0% to 15% mol DMF at 21 °C. (a) All radius evolution curves indicate IC thinning followed by EC thinning, delineated by the horizontal dotted line at $R/R_0 = 0.1$. The magnitude of the slope in the EC region decreases while the duration of the EC region increases with DMF content, indicating increasing solution elasticity. Dashed black lines denote fits to eq. 2. (b) Slender, cylindrical fluid filaments form prior to break up across all solutions ($R/R_0 \leq 0.1$), characteristic of EC behavior. The beads on a string instability forms for solutions with 5% to 15% mol DMF. The increasing prominence of the beads with DMF content reflects increasing solution elasticity.

Following the IC region, the radius evolution curves display a distinct exponential thinning regime, which is characteristic of elastocapillary (EC) thinning behavior (Figure 2a); these curves are shifted by t_c, the time at which the IC thinning behavior transitions to EC thinning behavior. Strikingly, the EC region becomes more pronounced – i.e. the slope decreases in magnitude while the duration increases – as DMF content is increased from 0% up to 15% mol, suggesting increasing solution elasticity (Figure 2a). This elasticity is also reflected in the distinct slender, cylindrical, and axisymmetric shape of the fluid filament prior to break up in all solutions (Figure 2b, $R/R_0 \leq 0.1$). Moreover, the beads on a string elastic instability appears with the addition of DMF. A greater number of beads form

along the filament as DMF content is increased from 5% to 15% mol, reflecting increasing chain extensibility.[53] Assuming a single polymer relaxation mode, the solution elasticity can be quantified by the extensional relaxation time λ_E, determined by fitting the exponential thinning regime to the EC model:[50,54]

$$\frac{R_{min}}{R_0} \approx \left(\frac{G_E R_0}{2\sigma}\right)^{1/3} \exp\left[-t/3\lambda_E\right] \tag{2}$$

where G_E is the elastic modulus and σ is the fluid surface tension. As previously reported by Zhang and Calabrese[18], the beads on a string instability gives rise to multiple sub-regions within the greater EC thinning region that correspond to traditional EC thinning, bead formation, and filament thinning between beads. As such, for the comparisons in this study, eq. 2 is only fit to the EC region prior to bead formation, resulting in the fits shown in Figure 2a and the extensional relaxation times λ_E in Table 1. The same trends persist when the entire EC region is fit instead, shown in SI.3.3.

Table 1: Shear and extensional rheology parameters for 0.5% wt PNIPAM solutions with varying DMF content.

DMF content [% mol]	η_0 [mPa · s]	λ_E [ms]	Δt_{EC} [ms]
0	2.0	0.27 ± 0.04	0.68 ± 0.16
5	3.0	1.4 ± 0.4	3.8 ± 1.4
10	3.6	4.2 ± 1.2	22 ± 3
15	3.6	8.5 ± 1.8	64 ± 11
50	2.8	0.12 ± 0.01	0.68 ± 0.10
100	1.8	-	-

Despite the non-monotonic trend in cloud point temperature T_{CP} from 0% to 15% mol DMF, the extensional relaxation time λ_E increases monotonically by more than twenty-fold from 0.27 ± 0.04 ms to 8.5 ± 1.8 ms when DMF content is increased from 0% DMF to 15%

DMF (Table 1). This trend persists even after λ_E is normalized by solvent shear viscosity η_s to account for the fact that λ_E can also increase with solvent shear viscosity (Table S2).[55] The span of the EC region, $\Delta t_{EC} = t_b - t_c$, also increases dramatically from 0.68 ± 0.16 ms to 64 ± 11 ms in the same range (Table 1). Thus, Δt_{EC} is also directly proportional to DMF content and λ_E as expected.[56]

Extensional rheology of DMF-rich solutions

Interestingly, when DMF content is further increased to 50% mol – within the one-phase region of solutions exhibiting UCST behavior – the solution elasticity dramatically decreases. The radius evolution curve of PNIPAM in 50% mol DMF still exhibits two thinning regimes, but the prominence of the EC region is greatly diminished and the flow behavior is dominated by IC thinning (Figure 3a). When the radius evolution curve is shifted by the end of the initial thinning regime, t_c, and plotted on a log-log scale, the resulting linearized curve can be fit to a power law model with an exponent $n = 2/3$. This exponent is in accordance with the IC model (eq. 1) – as expected given $Oh \ll 1$ (Figure 3b, Table S1). This IC behavior is further corroborated by the characteristic conical fluid filament shape prior to break up (Figure 3c).[51,52,57]

The initial IC thinning regime is again followed by an EC regime, although the span Δt_{EC} is only 0.68 ± 0.10 ms. Fits to eq. 2 yield an extensional relaxation time of 0.11 ± 0.01 ms (Table 1). Note that the apparent plateau at $t \approx 4.7$ ms is an imaging artifact as the sessile droplet briefly obscures the minimum radius of the fluid filament. Nonetheless, the solution elasticity, albeit rather weak, is corroborated by the appearance of a slender, cylindrical fluid filament in the final frames just prior to break up (Figure 3c). Both Δt_{EC} and λ_E for

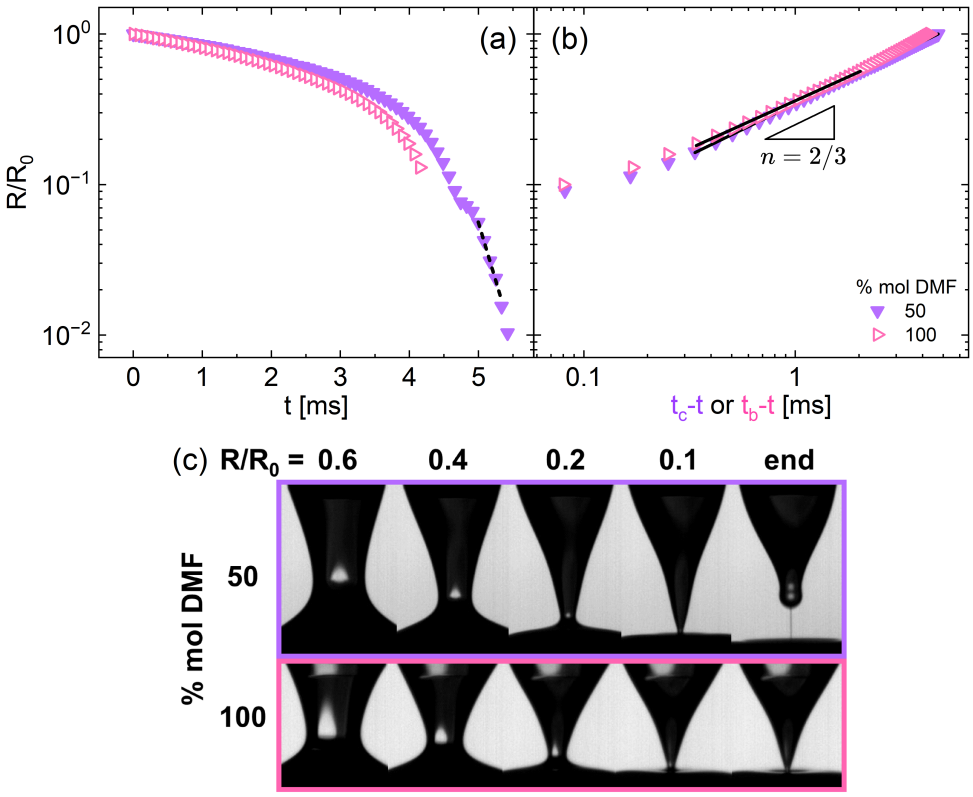

Figure 3: Self-thinning behavior of PNIPAM solutions with 50% and 100% DMF. (a) Radius evolution curves in the semi-log representation show that filament thinning is dominated by IC behavior in both cases, but 50% DMF solutions also exhibit a short EC region just prior to break up. Black dashed line denotes fit to eq. 2. (b) Linearized radius evolution curves are shifted by the time at which the IC region ends: t_c for 50% DMF and t_b for 100% DMF. These curves follow a power law scaling of exponent $n = 2/3$, in accordance with IC behavior (eq. 1). (c) The conical filament shape indicative of IC thinning is apparent in 2D images of PNIPAM solutions in both 50% and 100% DMF solutions. A slender, cylindrical filament is present in 50% DMF solutions just before break up, indicative of weak solution elasticity.

PNIPAM in 50% mol DMF are significantly reduced from the values for PNIPAM in 15% mol DMF, and are of the same order of magnitude as those for purely aqueous PNIPAM solutions.

Finally, in pure DMF solvent, PNIPAM solution elasticity completely diminishes. Here, the solution exhibits inertiocapillary thinning behavior only, and the radius evolution curve closely follows that of PNIPAM in 50% mol DMF (Figure 3a). The linearized radius evolution

curve exhibits the characteristic $n = 2/3$ power law scaling of IC thinning (Figure 3b). As expected, the fluid filament forms the distinctive conical shape prior to break up (Figure 3c).

Effect of DMF content on shear rheology of PNIPAM solutions

In contrast to observations in extensional rheology, the shear flow behavior of PNIPAM does not vary significantly with DMF content. Steady shear flow curves exhibit nearly Newtonian flow behavior wherein the shear viscosity, η, of all PNIPAM solutions ($c = 0.5\%$ wt) is largely invariant with shear rate, $\dot{\gamma}$, across all examined DMF concentrations (Figure 4a). The zero-shear viscosity, η_0, varies non-monotonically with solvent composition, exhibiting a maximum at a solvent composition of 15% mol DMF (Table 1). This trend in η_0 simply mirrors the variation in solvent viscosity as a function of DMF content in DMF/water mixtures (Figure S8).[58,59]

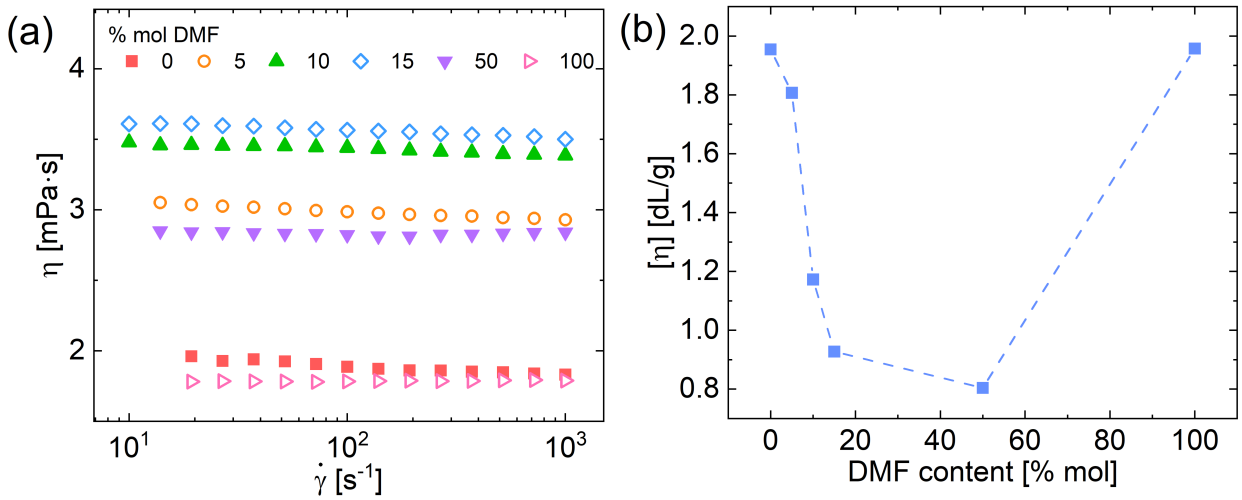

Figure 4: (a) Steady shear rheology for 0.5% wt PNIPAM solutions with varying DMF content shows nearly Newtonian behavior across all solutions. Zero-shear viscosities vary in accordance with solvent viscosities of DMF/water mixtures[58,59] (Table 1). (b) Intrinsic viscosity, $[\eta]$, of PNIPAM solutions decreases most steeply from 0% to 15% mol DMF, reaches a minimum at 50% mol DMF, then returns to a value at 100% DMF comparable to that at 0% DMF.

Interestingly, the apparent intrinsic viscosity, $[\eta]$, varies non-monotonically with DMF content. Here, the zero-shear viscosity as a function of PNIPAM concentration was measured for each DMF composition, and $[\eta]$ was extracted from fits to the Fedors equation[60] (see SI.5.1). The intrinsic viscosity most sharply decreases from 0% to 15% mol DMF, exhibits a minimum at 50% mol DMF, then returns to a value at 100% mol DMF that is near that at 0% DMF.

A decrease in intrinsic viscosity is often attributed to the collapse of individual polymer chains as a result of decreasing solvent quality.[61] Thus, the non-monotonic variation in $[\eta]$ suggests that DMF addition decreases solvent quality and induces polymer collapse in water-rich solutions while DMF addition increases solvent quality and leads to polymer swelling in DMF-rich solutions. However, the solvent quality in this system is expected to remain good or improve with the addition of DMF – a slightly better solvent for PNIPAM than water[38,62] – even as PNIPAM exhibits cosolvent-induced collapse in the two-phase region (Table S5).[31,38,63] As such, the cononsolvency behavior and underlying change in microstructure in PNIPAM/DMF/water systems appears to be decoupled from solvent quality, as previously suggested by Zhu and Chen[38].

In solution extensional rheology measurements, an increase in solvent quality is expected to result in an increase in the extensional relaxation time.[64–66] As λ_E varies non-monotonically while solvent quality remains good or slightly improves with DMF content (Table S5), varying solvent quality is unlikely to be the primary driver of the unique extensional rheological behavior in PNIPAM/DMF/water solutions. The variation in PNIPAM microstructure with DMF content indicated by intrinsic viscosities, however, does align with

findings from Zhu and Chen[38], thus the proposed impact on solution extensional flow behavior is further discussed below.

Notably, this change in intrinsic viscosity with DMF content implies that the overlap concentration c^*, estimated as $c^* \sim 1/[\eta]$, also changes with DMF content (Table S3). As such, at the fixed PNIPAM concentration of 0.5% wt examined here, c/c^* is not equal across DMF contents, with c/c^* near unity for some solutions and below unity for others. However, this pronounced increase in solution extensibility in the water-rich regime (Figure 2) also persists when all solutions are dilute (c = 0.1% wt PNIPAM, Figure S10). The persistence of this behavior in dilute polymer solutions – where c/c^* is far less than unity in all cases – suggests that the differences in solution extensibility are not simply due to differences in c/c^* with varying DMF content. As mentioned previously, the change in solvent viscosity with DMF content also does not account for these variations in solution extensional relaxation time. In summary, this unexpected increase in PNIPAM solution extensibility from 0% to 15% mol DMF cannot be explained by differences in solvent viscosity or solution concentration regime.

Proposed mechanism: DMF bridges PNIPAM chains

Prior studies have also reported cosolvent content-dependent solution extensional rheology for a variety of polymers. For example, aqueous solutions of charged polymers such as poly(acrylic acid) exhibit varying extensional relaxation times with isopropanol (IPA) concentration.[34] Khandavalli et al.[34] hypothesized that the changes in λ_E with IPA content could arise from enhanced inter-chain attractive interactions in extensional flows and changing electrostatic interactions that affect coil conformation (compact vs. more extended). Ad-

ditionally, the extensional rheology of aqueous hydrophobically associating alkali-swellable emulsion (HASE) polymer solutions varies with ethanol content, where λ_E increases with increasing ethanol fraction up to 60%. In HASE solutions, the changes in extensional rheology are attributed to variations in solvent quality and aggregate size as a function of ethanol content.[67] Finally, aqueous solutions of neutral polymers such as poly(ethylene oxide) also exhibit varying λ_E with acetonitrile content; these changes in extensional rheology were briefly attributed to competing hydrogen bonding interactions in polymer/cosolvent/water mixtures.[68] The common denominator across all aforementioned studies, despite differences in polymer chemistry, is the presence of interactions among polymer chains, solvent molecules, and cosolvent molecules that change with cosolvent content.

For PNIPAM/DMF/water systems, hydrogen bonding and hydrophobic interactions between PNIPAM chains and DMF molecules are thought to dictate solution properties and microstructure at low and intermediate DMF contents.[30,38] Zhu and Chen[38] reported preferential PNIPAM-DMF interactions, supported by Hansen solubility parameters that are closer for PNIPAM and DMF than PNIPAM and water.[62] As a result of these preferential interactions, the authors showed computationally that the number of non-bridging DMF molecules associating with PNIPAM chains generally increases with DMF content from 0% to 100% mol DMF. Notably, the number of associating DMF molecules that also bridge PNIPAM chains – thus forming physical crosslinks – increases with DMF content in the water-rich regime, exhibiting a maximum at intermediate DMF concentrations. This region of maximum number of bridging DMF molecules corresponds to the observed two-phase region wherein the PNIPAM microgels collapse. Such bridging of PNIPAM chains – or physical crosslinking –

by cosolvent molecules as a result of preferential hydrogen bonding and hydrophobic associations has also been reported in aqueous PNIPAM solutions with methanol,[31,69] ethanol,[70] urea,[71,72] and DMSO[73] cosolvents, and the mechanism is often proposed as the origin of cononsolvency in these systems.

In the DMF-rich regime, the number of bridging DMF molecules decreases and reaches a plateau as DMF content increases.[38] In this regime, DMF molecules disrupt the tetrahedral water network, likely impeding the hydration of PNIPAM chains.[39,74,75] Additionally, PNIPAM/DMF/water solutions become dominated by dipole-dipole interactions due to the high DMF content,[30] thus contributing to the loss of site-specific, hydrogen bonding-mediated bridging interactions between DMF and PNIPAM chains.

Based on the aforementioned studies, the evolution of the extensional relaxation time with of DMF content herein is proposed to result mainly from changes in the preferential hydrogen bonding interactions between PNIPAM chains and DMF cosolvent molecules as well as the resulting effect on PNIPAM microstructure. At low DMF contents, the number of bridging DMF molecules and λ_E both increase from 0% to 15% mol DMF.[38] At high DMF contents, the number of bridging DMF molecules diminishes[38] while λ_E significantly decreases. As such, bridging DMF molecules are proposed to act as physical crosslinks that increase the apparent molecular weight of PNIPAM in solution, resulting in the observed variation in PNIPAM/DMF/water solution extensional rheology.

Light scattering measurements support bridging mechanism

To explore the bridging hypothesis, the microstructure of PNIPAM solutions was probed by measuring the hydrodynamic radius, R_h, using dynamic light scattering and radius of

gyration, R_g, using static light scattering (Figure 5a). Results are reported for solutions with $c = 0.1\%$ wt PNIPAM, well below the lowest estimated overlap concentration of 0.5% wt determined from $c^* \sim 1/[\eta]$ (see Table S3 for c^* values and SI.7.2 for DLS at $c = 0.5\%$ wt). The hydrodynamic radius increases from 33.9 nm ± 1.0 nm to 38.4 nm ± 1.9 nm as DMF content increases from 0% to 15% mol DMF. In the DMF-rich regime, R_h instead decreases, to <30 nm in solutions with 50% and 100% mol DMF. On the other hand, the R_g is within uncertainty from 0% to 15% mol and then increases with DMF content up to 100% DMF. Note that these values of R_g and R_h in the one-phase regions support a mechanism that is distinct from the conformational collapse and aggregation of PNIPAM chains at temperatures above the LCST (two-phase region). Here, both R_g and R_h range from 28 nm to 40 nm in the one-phase regions while R_h of PNIPAM in 5% mol DMF/water above the LCST (i.e. collapsed and aggregated) was previously reported by Linn et al.[33] to be ∼200 nm.

Notably, the hydrodynamic radius increases with DMF content over the same range in which the extensional relaxation time increases. This increase in R_h from 0% to 15% mol DMF suggests increasing DMF adsorption to PNIPAM as both the number of non-bridging and the number of bridging DMF molecules should increase in this range.[38] Based on this evidence, we propose that the bridging DMF molecules in this regime form larger, physically associated PNIPAM networks that can behave as chains with higher apparent molecular weights, thus increasing the apparent chain extensibility. Note that the increase in hydrodynamic radius with increasing DMF content herein is distinct from prior measurements of chemically crosslinked PNIPAM microgels in DMF/water,[38] where R_h decreases with in-

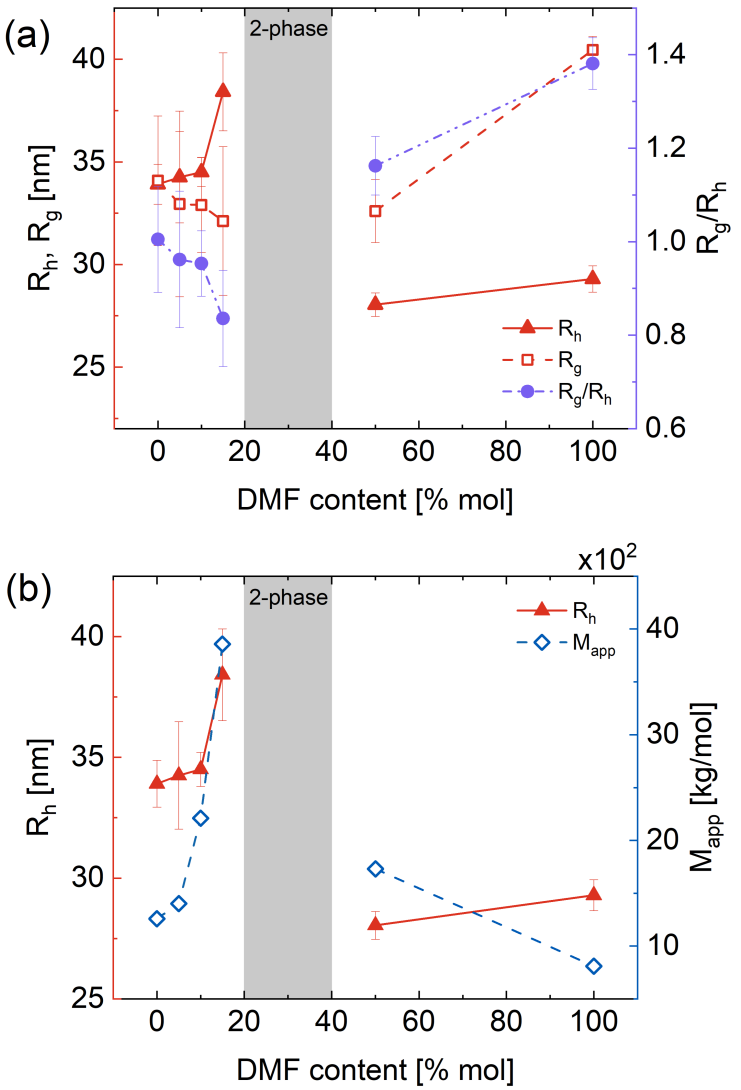

Figure 5: (a) Coil size measurements and shape factor R_g/R_h as a function of DMF content for 0.1% wt PNIPAM solutions ($c < c^*$). Hydrodynamic radius (R_h) exhibits a maximum while radius of gyration (R_g) exhibits a minimum at 15% mol DMF, suggesting changes in solvation and underlying microstructure. The shape factor reflects these changes, decreasing from 0% to 15% mol DMF to reflect the formation of denser aggregates due to DMF bridging. The shape factor then increases with DMF content up to 100% DMF, reflecting increasing solvation by non-bridging DMF and a return to Gaussian coils in solution. (b) Apparent molecular weight (M_{app}) increases from 0% to 15% mol DMF as DMF bridging increases, then decreases from 15% to 100% mol DMF as chains become solvated again. Hydrodynamic radius R_h is co-plotted for reference.

creasing DMF content from 0% to 15% mol DMF. This difference in the evolution of R_h is likely due to differences between the freely-moving, linear PNIPAM chains studied herein

and the chemically cross-linked PNIPAM microgel particles studied by Zhu and Chen[38]. As PNIPAM microgel particles are often colloidally-stable in both the swollen and collapsed states,[76,77] the decrease in R_h of PNIPAM microgels reflects the decrease in hydrodynamic volume of dispersed individual particles, which Zhu and Chen[38] attribute to intra-particle DMF-bridging. Due to the constraints of the chemical crosslinks and the colloidal stability of these microgel suspensions, R_h should change concomitantly with R_g in these types of systems. In contrast, linear PNIPAM chains do not have the same constraints imparted by chemical crosslinking, and the evolution in R_h reflects the behavior of single free chains or several associated chains. Thus here, R_g and R_h can evolve differently with DMF content. Therefore, for the solution of linear chains in this work, we propose that increasing DMF-induced bridging between free PNIPAM chains – which is not possible for chemically crosslinked microgels – results in the observed increase in R_h from 0% to 15% mol DMF.

In 50% and 100% mol DMF, the hydrodynamic radius decreases to values near that of R_h measured in 0% mol DMF (Figure 5a). This decrease in R_h is attributed to increasing solvation of PNIPAM chains by non-bridging DMF molecules in the DMF-rich region. As a result, the PNIPAM chains exist in solution more as individual chains – closer to the conformation of PNIPAM in pure water – rather than larger networks or aggregates. In this event, the apparent molecular weight of chains would decrease, resulting in a significant decrease in solution elasticity – as is observed in the extensional rheology measurements. This idea is supported by: (1) the prominence of non-site-specific dipole-dipole interactions among PNIPAM and DMF in this regime[30] and (2) the monotonic increase in associating, non-bridging DMF molecules coupled with the decreasing number of associating, bridging

DMF molecules in PNIPAM microgel solutions with $\geq 50\%$ mol DMF.[38]

To demonstrate that DMF content affects the apparent molecular weight of PNIPAM in solution, the following relation is invoked, derived from the Einstein equation for effective viscosity of a dilute suspension of particles of volume fraction ϕ:[78]

$$[\eta] = \frac{5N_{Av}}{2}\frac{V_h}{M_{app}} = \frac{5N_{Av}}{2M_{app}}\frac{4\pi R_h^3}{3} \tag{3}$$

where N_{Av} is Avogadro's number, V_h is the hydrodynamic volume, and M_{app} is the apparent molecular weight; the volume fraction is defined as $\phi = c/M_{app}N_{Av}V_h$. Using R_h from DLS measurements and $[\eta]$ from shear rheology, an estimate for M_{app} is calculated, which is plotted as a function of DMF content in Figure 5b. The hydrodynamic radius is co-plotted for reference. The apparent molecular weight increases from 0% to 15% mol DMF in accordance with the increase in R_h and λ_E over the same range. Then, M_{app} decreases with DMF content at 50% and 100% mol DMF, the same range in which R_h and λ_E decrease. Notably, the estimated apparent molecular weights are approximately $1 \cdot 10^6$ g/mol in 0% mol DMF and $8 \cdot 10^5$ g/mol in 100% mol DMF – comparable to the measured weight-average molecular weight of the PNIPAM used in this study ($M_w \sim 9 \cdot 10^5$ g/mol). Prior studies have shown that M_w rather than the number-average molecular weight (M_n) most significantly impacts the extensional relaxation time of polymer solutions,[79,80] thus lending credence to these calculations. As such, these calculations support the idea that an increase in DMF bridging molecules manifests in an increase in PNIPAM apparent molecular weight in the water-rich regime. At higher DMF concentrations, PNIPAM chains become solvated by non-bridging DMF molecules via dipole-dipole interactions, decreasing M_{app}.

Considering the shape factor, R_g/R_h, helps rationalize the apparent discrepancy between individual values of R_g and R_h. A shape factor of 1.5 corresponds to a Gaussian coil while a shape factor of 0.78 corresponds to a hard sphere.[78,81] As shown in Figure 5a, R_g/R_h decreases slightly from 1.0 at 0% DMF to a value of 0.8 at 15% mol DMF, reflecting the transition from a coil in pure water towards a more compact sphere in the presence of 15% mol DMF. Considering the proposed mechanism of DMF-mediated interchain bridging between 0% and 15% mol DMF, this decrease in R_g/R_h further evidences the formation of PNIPAM aggregates that are physically crosslinked by DMF molecules. A similar decrease in R_g/R_h occurs upon an increase in chemical crosslinker fraction in PNIPAM microgels[82–84] and the number of associative groups in hydrophobically-associating polyacrylamides.[85] The hard sphere value of the shape factor herein may indicate denser PNIPAM aggregates or non-uniform density throughout the aggregates. For example, in chemically crosslinked PNIPAM microgels, low values of R_g/R_h have been attributed to a microstructure wherein a denser, more crosslinked core is surrounded by a shell of long, loosely crosslinked dangling chains.[82–84] The formation of denser PNIPAM aggregates indicated by the shape factor also aligns with the decrease in the apparent intrinsic viscosity from 0% to 15% mol DMF (Figure 4b). In the DMF-rich regime, R_g/R_h increases from 0.8 at 15% DMF to 1.4 at 100% DMF, indicating a transition from more compact spheres back towards Gaussian coils, further supporting the proposed solvation of PNIPAM chains by non-bridging DMF molecules in DMF-rich solvent. The apparent $[\eta]$ also increases in this range, in agreement with the proposed mechanism based on R_g/R_h.

Discussion

Although conducted under quiescent conditions, light scattering measurements provide significant insight into the evolution of PNIPAM-DMF interactions and consequent PNIPAM microstructures as a function of DMF content. Here, a mechanism by which DMF-mediated PNIPAM interactions affect the extensional rheology of PNIPAM/DMF/water solutions is proposed. At 0% DMF, single PNIPAM chains or small clusters of few PNIPAM chains are being stretched in extensional flows, resulting in minimal elasticity (Figure 6a). As discussed previously, M_{app} increases from 0% to 15% mol DMF as a result of DMF bridging associations that effectively act as physical crosslinks. Thus, as DMF content is increased, increasingly associated chains with increasing M_{app} are stretched in concert, resulting in greater extensibility – just like λ_E increases with molecular weight in binary solutions of non-associating neutral polymers.[55,80] The observed increase in extensional relaxation time with interchain bridging herein is also analogous to the increase in λ_E with the presence or number of associative groups (i.e. "stickers") in associative polymer solutions.[86–88] Notably, these associative interactions may be exacerbated in extensional flows as polymer chains interact more strongly with each other in extensional flows than in quiescent conditions due to larger pervaded volumes in the stretched state,[55,89,90] thus amplifying effects on λ_E.

At 50% and 100% DMF, M_{app} decreases as the number of bridging DMF molecules diminishes and non-bridging DMF increasingly solvates PNIPAM chains (Figure 6b). At 50% mol DMF, minimally associated chains are being stretched in extensional flow, resulting in the decrease in solution elasticity and relatively short extensional relaxation time observed. At 100% DMF, single PNIPAM chains solvated by non-bridging DMF molecules are being

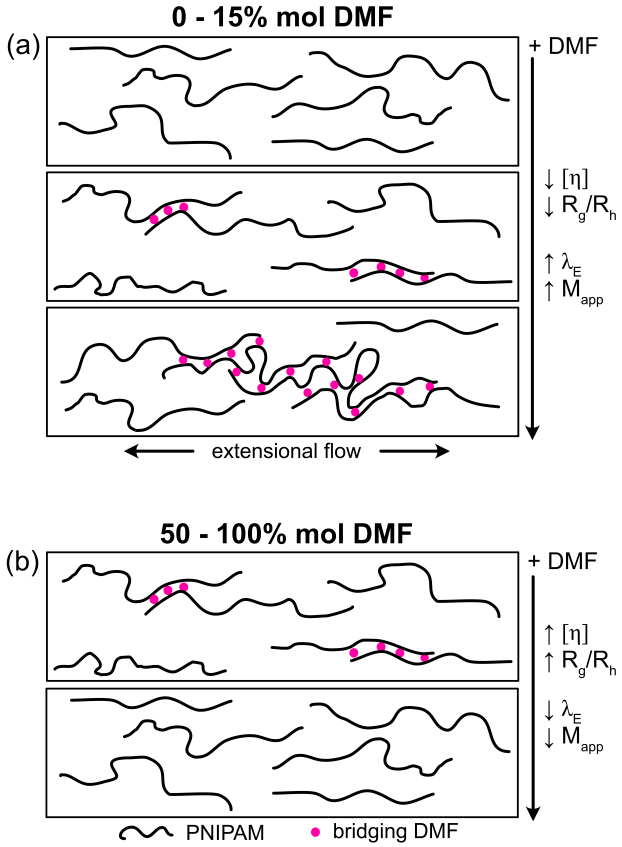

Figure 6: Summary of trends and proposed mechanisms in extensional flow as a function of DMF content. (a) As DMF content increases from 0% to 15% mol DMF in the water-rich, one-phase regime, intrinsic viscosity $[\eta]$ and the shape factor R_g/R_h increase, reflecting a microstructural change as DMF molecules increasingly associate with and bridge PNIPAM chains. Consequently, M_{app} increases, which in turn leads to the observed increase in λ_E. (c) As DMF content increases from 50% to 100% mol DMF in the DMF-rich, one-phase regime, $[\eta]$ and R_g/R_h increase as dipole-dipole interactions dominate, and PNIPAM chains are increasingly solvated by non-bridging DMF molecules. Consequently, M_{app} decreases, resulting in the decrease in λ_E.

stretched, resulting once again in minimal solution elasticity.

The bridging mechanism at low and intermediate DMF content is likely aided by bulk solvent structure. Hydrophobic hydration – where water forms a structured hydration shell around hydrophobic moieties such as the PNIPAM isopropyl group – is known to play a critical role in aqueous PNIPAM solution phase behavior.[47] Similarly, in DMF/water solvent mixtures, DMF addition enhances the tetrahedral structure of water at low DMF incorpo-

ration ($\lesssim$13.5% mol DMF[39]) due to the introduction of hydrophobic methyl groups.[39,74,75] Thus, in ternary PNIPAM/DMF/water solutions, the presence of both PNIPAM isopropyl groups and DMF methyl groups at low DMF concentrations likely enhance the tetrahedral structuring of water, driving some PNIPAM chains together as the release of water from the hydration shell is entropically favorable.[47,91–93] The closer proximity of PNIPAM chains driven together by hydrophobic hydration can make the bridging of PNIPAM chains via preferential PNIPAM-DMF interactions more facile. In the DMF-rich region, DMF molecules disrupt the tetrahedral structure of water, likely impeding the hydration of PNIPAM chains.[39,74,75] Instead, dipole-dipole interactions between PNIPAM and DMF dominate due to the large fraction of DMF molecules present, lending to increased solvation of PNIPAM chains by non-bridging DMF molecules.[30]

Conclusions

This work reveals that the extensional rheology of aqueous PNIPAM solutions varies unexpectedly with DMF cosolvent content. In the one-phase, water-rich regime, solutions exhibit elastocapillary thinning behavior, and the extensional relaxation time increases by more than twenty-fold as DMF content increases. Meanwhile, in this same range, the cloud point temperature exhibits a maximum, suggesting that the mechanism behind the extensional rheology is distinct from LCST behavior. Instead, this remarkable increase in solution elasticity is attributed to preferential hydrogen bonding interactions between DMF cosolvent molecules and PNIPAM chains wherein DMF molecules bridge PNIPAM chains, forming physically crosslinked aggregates/networks – a mechanism proposed previously in compu-

tational studies. This inter-chain bridging is proposed to increase the apparent molecular weight of PNIPAM, resulting in a concomitant increase in solution extensibility. This phenomenon can be exacerbated in extensional flows wherein inter-chain interactions are enhanced due to the higher pervaded volumes of stretched polymer chains. As DMF content is increased further to 50% and 100% mol in the DMF-rich one-phase region, solution elasticity decreases significantly, and filament thinning is dominated by inertiocapillary behavior. The reduced solution extensibility in DMF-rich solutions results from a reduction in the number of inter-chain bridging DMF molecules and an increase in non-bridging DMF solvation of PNIPAM chains.

Overall, this study provides valuable experimental insight into the complex effects of DMF – a cosolvent with preferential affinity to PNIPAM – addition on the extensional rheology of PNIPAM solutions. The results herein demonstrate that interactions among polymer, solvent, and cosolvent can have significant effects on polymer microstructure in solution, which tends to impact extensional flow behavior more dramatically than shear flow behavior. Therefore, these interactions must be considered when designing polymer-containing formulations that are amenable to extensional flow-dominated processes such as spraying and atomization, coating, and fiber spinning. For example here, the addition of $\geq$50% mol DMF would enable a high molecular weight polymer ($M_w \approx 1{\cdot}10^6$ g/mol) to be processed much more readily in spraying and coating operations due to significantly reduced elasticity. Nevertheless, additional spectroscopic studies are needed to directly probe interactions among PNIPAM, DMF, and water molecules in solution. Molecular dynamics simulations may also aid in further understanding the DMF bridging mechanism. The generality of

the findings herein should be further assessed to probe if other cosolvents with preferential affinity to PNIPAM, such as methanol, induce the same extensional rheological behavior. Ultimately, developing fundamental understanding of the interactions in these ternary polymer solutions informs the use of cosolvent addition as a strategy to tune polymer processability for applications ranging from spraying and atomization to fiber spinning, thus enabling the design of processable polymer-containing formulations.

Author contributions

CRediT: Diana Y. Zhang - formal analysis, investigation, methodology, validation, visualization, funding acquisition, writing - original draft. Alec J. Schwendinger - formal analysis, investigation, validation. Michelle A. Calabrese - conceptualization, funding acquisition, project administration, resources, supervision, writing - review & editing.

Acknowledgement

This material is based upon work supported by the National Science Foundation Graduate Research Fellowship under Grant No. 2237827 as well as the National Science Foundation under Award Number DMR-2323989. Any opinion, findings, and conclusions or recommendations expressed in this material are those of the authors and do not necessarily reflect the views of the National Science Foundation. The authors also acknowledge support from the University of Minnesota College of Science and Engineering and Office of Undergraduate Research. The authors thank the Anton Paar VIP program for the shear rheometer used in this work. The authors thank Benjamin Robertson, Jason Linn, Soumi Das, and Timothy Lodge for insightful discussions and helpful suggestions.

Supporting Information Available

See supplementary information for PNIPAM characterization, representative of cloud point data, additional fits to extensional rheology data, control DoS experiments, solvent viscosities, intrinsic viscosity and overlap concentration calculations, solvent quality estimates, DoS measurements of lower concentration PNIPAM solutions, additional DLS data and analysis, and additional SLS data and analysis.

Notes

The authors declare no competing financial interests.

References

(1) Matsuguchi, M.; Tada, A. Fabrication of poly(N-isopropylacrylamide) nanoparticles using a simple spray-coating method and applications for a QCM-based HCl gas sensor coating. *Sens. Actuators B Chem.* **2017**, *251*, 821–827.

(2) Yakushiji, T.; Sakai, K.; Kikuchi, A.; Aoyagi, T.; Sakurai, Y.; Okano, T. Graft Architectural Effects on Thermoresponsive Wettability Changes of Poly(*N* -isopropylacrylamide)-Modified Surfaces. *Langmuir* **1998**, *14*, 4657–4662.

(3) Chu, L.-Y.; Niitsuma, T.; Yamaguchi, T.; Nakao, S.-i. Thermoresponsive transport through porous membranes with grafted PNIPAM gates. *AIChE J.* **2003**, *49*, 896–909.

(4) Chen, R.; Wang, H.; Doucet, M.; Browning, J. F.; Su, X. Thermo-Electro-Responsive

Redox-Copolymers for Amplified Solvation, Morphological Control, and Tunable Ion Interactions. *JACS Au* **2023**, *3*, 3333–3344.

(5) Ding, J.-J.; Zhu, J.; Li, Y.-X.; Liu, X.-Q.; Sun, L.-B. Smart Adsorbents Functionalized with Thermoresponsive Polymers for Selective Adsorption and Energy-Saving Regeneration. *Ind. Eng. Chem. Res.* **2017**, *56*, 4341–4349.

(6) Xu, X.; Bizmark, N.; Christie, K. S. S.; Datta, S. S.; Ren, Z. J.; Priestley, R. D. Thermoresponsive Polymers for Water Treatment and Collection. *Macromolecules* **2022**, *55*, 1894–1909.

(7) Gadore, V.; Ahmaruzzaman, M. Smart materials for remediation of aqueous environmental contaminants. *J. Environ. Chem. Eng.* **2021**, *9*, 106486.

(8) Heskins, M.; Guillet, J. E. Solution Properties of Poly(N-isopropylacrylamide). *J. Macromol. Sci. Chem. A* **1968**, *2*, 1441–1455.

(9) Schild, H. Poly(N-isopropylacrylamide): experiment, theory and application. *Prog. Polym. Sci.* **1992**, *17*, 163–249.

(10) Liu, Y.; Waterhouse, G. I. N.; Jiang, X.; Zhang, Z.; Yu, L. Smart antibiofouling composite coatings based on photothermally-active polyaniline and thermo-responsive poly(N-isopropylacrylamide). *Chem. Eng. J.* **2024**, *490*, 151669.

(11) Ganesh, V. A.; Ranganath, A. S.; Sridhar, R.; Raut, H. K.; Jayaraman, S.; Sahay, R.; Ramakrishna, S.; Baji, A. Cellulose Acetate–Poly(N-isopropylacrylamide)-Based Func-

tional Surfaces with Temperature-Triggered Switchable Wettability. *Macromol. Rapid Commun.* **2015**, *36*, 1368–1373.

(12) Götz, T.; Landzettel, J.; Schiestel, T. Thermo-responsive mixed-matrix hollow fiber membranes. *J. Appl. Polym. Sci.* **2021**, *138*, 50787.

(13) Li, H.; Zhang, G.; Deng, L.; Sun, R.; Ou-Yang, X. Thermally responsive behaviour of the electrical resistance of electrospun P(NIPAm-co-NMA)/Ag composite nanofibers. *RSC Adv.* **2014**, *5*, 6413–6418.

(14) Fernando, R. H. Erratum to "Rheology parameters controlling spray atomization and roll misting behavior of waterborne coatings" [Prog. Org. Coat. 40 (2000) 35–38]. *Prog. Org. Coat.* **2001**, *42*, 284–288.

(15) Yoon, K.; Hsiao, B. S.; Chu, B. Functional nanofibers for environmental applications. *J. Mater. Chem.* **2008**, *18*, 5326–5334.

(16) Khandavalli, S.; Sharma-Nene, N.; Kabir, S.; Sur, S.; Rothstein, J. P.; Neyerlin, K. C.; Mauger, S. A.; Ulsh, M. Toward Optimizing Electrospun Nanofiber Fuel Cell Catalyst Layers: Polymer–Particle Interactions and Spinnability. *ACS Appl. Polym. Mater.* **2021**, *3*, 2374–2384.

(17) Kang, S. K.; Ho, D. H.; Lee, C. H.; Lim, H. S.; Cho, J. H. Actively Operable Thermoresponsive Smart Windows for Reducing Energy Consumption. *ACS Appl. Mater. Interfaces.* **2020**, *12*, 33838–33845.

(18) Zhang, D. Y.; Calabrese, M. A. Temperature-controlled dripping-onto-substrate (DoS) extensional rheometry of polymer micelle solutions. *Soft Matter* **2022**, *18*, 3993–4008.

(19) Dinic, J.; Biagioli, M.; Sharma, V. Pinch-off dynamics and extensional relaxation times of intrinsically semi-dilute polymer solutions characterized by dripping-onto-substrate rheometry. *J. Polym. Sci., Part B: Polym. Phys.* **2017**, *55*, 1692–1704.

(20) Matta, J. E.; Tytus, R. P.; Harris, J. L. Aerodynamic Atomization of Polymeric Solutions. *Chem. Eng. Commun.* **1983**, *19*, 191–204.

(21) Desai, K.; Kit, K. Effect of spinning temperature and blend ratios on electrospun chitosan/poly(acrylamide) blends fibers. *Polymer* **2008**, *49*, 4046–4050.

(22) Fujishige, S.; Kubota, K.; Ando, I. Phase transition of aqueous solutions of poly(N-isopropylacrylamide) and poly(N-isopropylmethacrylamide). *J. Phys. Chem.* **1989**, *93*, 3311–3313.

(23) Halperin, A.; Kröger, M.; Winnik, F. M. Poly (N-isopropylacrylamide) phase diagrams: fifty years of research. *Angew. Chem. Int. Ed.* **2015**, *54*, 15342–15367.

(24) Ohnsorg, M. L.; Ting, J. M.; Jones, S. D.; Jung, S.; Bates, F. S.; Reineke, T. M. Tuning PNIPAm self-assembly and thermoresponse: roles of hydrophobic end-groups and hydrophilic comonomer. *Polym. Chem.* **2019**, *10*, 3469–3479.

(25) Zhang, Y.; Wang, P.; Chen, R. Effect of the macromolecular architecture on the thermoresponsive behavior of poly(N-isopropylacrylamide) in copolymers with poly(N,N-

dimethylacrylamide) in aqueous solutions: Block vs random copolymers. *React. Funct. Polym.* **2022**, *171*, 105150.

(26) de Oliveira, T. E.; Mukherji, D.; Kremer, K.; Netz, P. A. Effects of stereochemistry and copolymerization on the LCST of PNIPAm. *J. Chem. Phys.* **2017**, *146*, 034904.

(27) Patel, T.; Ghosh, G.; Yusa, S.-i.; Bahadur, P. Solution Behavior of Poly(n-Isopropylacrylamide) in Water: Effect of Additives. *J. Disper. Sci. Technol.* **2011**, *32*, 1111–1118.

(28) Umapathi, R.; Madhusudhana Reddy, P.; Rani, A.; Venkatesu, P. Influence of additives on thermoresponsive polymers in aqueous media: a case study of poly(N -isopropylacrylamide). *Phys. Chem. Chem. Phys.* **2018**, *20*, 9717–9744.

(29) Narang, P.; Venkatesu, P. An efficient study to reach physiological temperature with poly(N-isopropylacrylamide) in presence of two differently behaving additives. *J. Colloid Interface Sci.* **2019**, *538*, 62–74.

(30) Costa, R. O.; Freitas, R. F. Phase behavior of poly(N-isopropylacrylamide) in binary aqueous solutions. *Polymer* **2002**, *43*, 5879–5885.

(31) Mukherji, D.; Wagner, M.; Watson, M. D.; Winzen, S.; de Oliveira, T. E.; Marques, C. M.; Kremer, K. Relating side chain organization of PNIPAm with its conformation in aqueous methanol. *Soft Matter* **2016**, *12*, 7995–8003.

(32) Mukherji, D.; Kremer, K. Coil–Globule–Coil Transition of PNIPAm in Aqueous

Methanol: Coupling All-Atom Simulations to Semi-Grand Canonical Coarse-Grained Reservoir. *Macromolecules* **2013**, *46*, 9158–9163.

(33) Linn, J. D.; Rodriguez, F. A.; Calabrese, M. A. Cosolvent incorporation modulates the thermal and structural response of PNIPAM/silyl methacrylate copolymers. *Soft Matter* **2024**, *20*, 3322–3336.

(34) Khandavalli, S.; Chen, Y.; Sharma-Nene, N.; Rajan, K. S.; Sur, S.; Rothstein, J. P.; Reeves, K. S.; Cullen, D. A.; Neyerlin, K. C.; Mauger, S. A.; Ulsh, M. Effect of isopropanol cosolvent on the rheology and spinnability of aqueous polyacrylic acid solutions. *J. Polym. Sci.* **2023**, *61*, 1495–1512.

(35) Merchiers, J.; Reddy, N. K.; Sharma, V. Extensibility-Enriched Spinnability and Enhanced Sorption and Strength of Centrifugally Spun Polystyrene Fiber Mats. *Macromolecules* **2022**, *55*, 942–955.

(36) Bharadwaj, S.; Niebuur, B.-J.; Nothdurft, K.; Richtering, W.; van der Vegt, N. F. A.; Papadakis, C. M. Cononsolvency of thermoresponsive polymers: where we are now and where we are going. *Soft Matter* **2022**, *18*, 2884–2909.

(37) Yu, Y.; Cruz, R. A. L. d. l.; D. Kieviet, B.; Gojzewski, H.; Pons, A.; Vancso, G. J.; Beer, S. d. Pick up, move and release of nanoparticles utilizing co-non-solvency of PNIPAM brushes. *Nanoscale* **2017**, *9*, 1670–1675.

(38) Zhu, P.-w.; Chen, L. Effects of cosolvent partitioning on conformational transitions and chain flexibility of thermoresponsive microgels. *Phys. Rev. E* **2019**, *99*, 022501.

(39) Yang, B.; Lang, H.; Liu, Z.; Wang, S.; Men, Z.; Sun, C. Three stages of hydrogen bonding network in DMF-water binary solution. *J. Mol. Liq.* **2021**, *324*, 114996.

(40) Neal, C. A. P.; Kresge, G. V.; Quan, M. C.; León, V.; Chibambo, N. O.; Calabrese, M. A. Effect of nanoparticle loading and magnetic field application on the thermodynamic, optical, and rheological behavior of thermoresponsive polymer solutions. *J. Vinyl Addit. Technol.* **2022**, *29*, 795–812.

(41) Osváth, Z.; Iván, B. The Dependence of the Cloud Point, Clearing Point, and Hysteresis of Poly(*N* -isopropylacrylamide) on Experimental Conditions: The Need for Standardization of Thermoresponsive Transition Determinations. *Macromol. Chem. Phys.* **2017**, *218*, 1600470.

(42) Neal, C. A.; Shetty, A. M.; Linn, J. D.; Quan, M. C.; Casas, J. D.; Calabrese, M. A. Magnetic field-dependent rheological behavior of thermoresponsive poly (N-isopropylacrylamide) solutions. *Rheol. Acta* **2024**, 1–20.

(43) Jakeš, J. Regularized Positive Exponential Sum (REPES) Program - A Way of Inverting Laplace Transform Data Obtained by Dynamic Light Scattering. *Collect. Czechoslov. Chem. Commun.* **1995**, *60*, 1781–1797.

(44) Dinic, J.; Zhang, Y.; Jimenez, L. N.; Sharma, V. Extensional Relaxation Times of Dilute, Aqueous Polymer Solutions. *ACS Macro Lett.* **2015**, *4*, 804–808.

(45) Lauser, K. T.; Rueter, A. L.; Calabrese, M. A. Small-volume extensional rheology of concentrated protein and protein-excipient solutions. *Soft Matter* **2021**, *17*, 9624–9635.

(46) Henschel, C.; Schanzenbach, D.; Laschewsky, A.; Ko, C.-H.; Papadakis, C. M.; Müller-Buschbaum, P. Thermoresponsive and co-nonsolvency behavior of poly(N-vinyl isobutyramide) and poly(N-isopropyl methacrylamide) as poly(N-isopropyl acrylamide) analogs in aqueous media. *Colloid Polym. Sci.* **2023**, *301*, 703–720.

(47) Bischofberger, I.; Calzolari, D. C. E.; De Los Rios, P.; Jelezarov, I.; Trappe, V. Hydrophobic hydration of poly-N-isopropyl acrylamide: a matter of the mean energetic state of water. *Sci. Rep.* **2014**, *4*, 4377.

(48) Philipp, M.; Kyriakos, K.; Silvi, L.; Lohstroh, W.; Petry, W.; Krüger, J. K.; Papadakis, C. M.; Müller-Buschbaum, P. From Molecular Dehydration to Excess Volumes of Phase-Separating PNIPAM Solutions. *J. Phys. Chem. B* **2014**, *118*, 4253–4260.

(49) Meier-Koll, A.; Pipich, V.; Busch, P.; Papadakis, C. M.; Müller-Buschbaum, P. Phase Separation in Semidilute Aqueous Poly(*N* -isopropylacrylamide) Solutions. *Langmuir* **2012**, *28*, 8791–8798.

(50) McKinley, G. H. Visco-elasto-capillary thinning and break-up of complex fluids. *Rheol. Rev.* **2005**, 1–48.

(51) Castrejón-Pita, J. R.; Castrejón-Pita, A. A.; Hinch, E. J.; Lister, J. R.; Hutchings, I. M. Self-similar breakup of near-inviscid liquids. *Phys. Rev. E* **2012**, *86*, 015301.

(52) Day, R. F.; Hinch, E. J.; Lister, J. R. Self-Similar Capillary Pinchoff of an Inviscid Fluid. *Phys. Rev. Lett.* **1998**, *80*, 704–707.

(53) Chang, H.-C.; Demekhin, E. A.; Kalaidin, E. Iterated stretching of viscoelastic jets. *Phys. Fluids* **1999**, *11*, 1717–1737.

(54) Entov, V.; Hinch, E. Effect of a spectrum of relaxation times on the capillary thinning of a filament of elastic liquid. *J. Non-Newton. Fluid Mech.* **1997**, *72*, 31–53.

(55) Sur, S.; Rothstein, J. Drop breakup dynamics of dilute polymer solutions: Effect of molecular weight, concentration, and viscosity. *J. Rheol.* **2018**, *62*, 1245–1259.

(56) Dinic, J.; Sharma, V. Macromolecular relaxation, strain, and extensibility determine elastocapillary thinning and extensional viscosity of polymer solutions. *Proc. Natl. Acad. Sci.* **2019**, *116*, 8766–8774.

(57) Peregrine, D. H.; Shoker, G.; Symon, A. The bifurcation of liquid bridges. *J. Fluid Mech.* **1990**, *212*, 25.

(58) Taniewska-Osinska, S.; Piekarska, A.; Kacperska, A. Viscosities of NaI in water-formamide and water-N,N-dimethylformamide mixtures from 5 to 45°C. *J. Solution Chem.* **1983**, *12*, 717–727.

(59) Aminabhavi, T. M.; Gopalakrishna, B. Density, Viscosity, Refractive Index, and Speed of Sound in Aqueous Mixtures of N,N-Dimethylformamide, Dimethyl Sulfoxide, N,N-Dimethylacetamide, Acetonitrile, Ethylene Glycol, Diethylene Glycol, 1,4-Dioxane, Tetrahydrofuran, 2-Methoxyethanol, and 2-Ethoxyethanol at 298.15 K. *J. Chem. Eng. Data* **1995**, *40*, 856–861.

(60) Fedors, R. F. An equation suitable for describing the viscosity of dilute to moderately concentrated polymer solutions. *Polymer* **1979**, *20*, 225–228.

(61) Marani, D.; Hjelm, J.; Wandel, M. Use of Intrinsic Viscosity for Evaluation of Polymer-Solvent Affinity. *Ann. T. Nord. Rheol. Soc.* **2013**, *21*, 255–262.

(62) Hansen, C. M. *Hansen solubility parameters : a user's handbook*; CRC Press: Boca Raton, FL, 2000.

(63) Mukherji, D.; Marques, C. M.; Kremer, K. Collapse in two good solvents, swelling in two poor solvents: defying the laws of polymer solubility? *J. Phys. Condens. Matter* **2018**, *30*, 024002.

(64) Kong, Y.; Manke, C. W.; Madden, W. G.; Schlijper, A. G. Effect of solvent quality on the conformation and relaxation of polymers via dissipative particle dynamics. *J. Chem. Phys.* **1997**, *107*, 592–602.

(65) Andrews, N. C.; Doufas, A. K.; McHugh, A. J. Effect of Solvent Quality on the Rheological and Rheooptical Properties of Flexible Polymer Solutions. *Macromolecules* **1998**, *31*, 3104–3108.

(66) Robertson, B. P.; Calabrese, M. A. Evaporation-controlled dripping-onto-substrate (DoS) extensional rheology of viscoelastic polymer solutions. *Sci. Rep.* **2022**, *12*, 4697.

(67) Kheirandish, S.; Guybaidullin, I.; Wohlleben, W.; Willenbacher, N. Shear and elongational flow behavior of acrylic thickener solutions: Part I: Effect of intermolecular aggregation. *Rheol. Acta* **2008**, *47*, 999–1013.

(68) Merchiers, J.; Slykas, C. L.; Martínez Narváez, C. D. V.; Buntinx, M.; Deferme, W.; Peeters, R.; Reddy, N. K.; Sharma, V. Fiber Engineering Trifecta of Spinnability, Morphology, and Properties: Centrifugally Spun versus Electrospun Fibers. *ACS Appl. Polym. Mater.* **2022**, *4*, 2022–2035.

(69) Kojima, H.; Tanaka, F.; Scherzinger, C.; Richtering, W. Temperature dependent phase behavior of PNIPAM microgels in mixed water/methanol solvents. *J. Polym. Sci., Part B: Polym. Phys.* **2013**, *51*, 1100–1111.

(70) Backes, S.; Krause, P.; Tabaka, W.; Witt, M. U.; Mukherji, D.; Kremer, K.; von Klitzing, R. Poly(N -isopropylacrylamide) Microgels under Alcoholic Intoxication: When a LCST Polymer Shows Swelling with Increasing Temperature. *ACS Macro Lett.* **2017**, *6*, 1042–1046.

(71) Wang, J.; Liu, B.; Ru, G.; Bai, J.; Feng, J. Effect of Urea on Phase Transition of Poly(N -isopropylacrylamide) and Poly(N , N -diethylacrylamide) Hydrogels: A Clue for Urea-Induced Denaturation. *Macromolecules* **2016**, *49*, 234–243.

(72) Sagle, L. B.; Zhang, Y.; Litosh, V. A.; Chen, X.; Cho, Y.; Cremer, P. S. Investigating the Hydrogen-Bonding Model of Urea Denaturation. *J. Am. Chem. Soc.* **2009**, *131*, 9304–9310.

(73) Yong, H.; Sommer, J.-U. Cononsolvency Effect: When the Hydrogen Bonding between a Polymer and a Cosolvent Matters. *Macromolecules* **2022**, *55*, 11034–11050.

(74) Lei, Y.; Li, H.; Pan, H.; Han, S. Structures and Hydrogen Bonding Analysis of *N* ,

N -Dimethylformamide and *N* , *N* -Dimethylformamide-Water Mixtures by Molecular Dynamics Simulations. *J. Phys. Chem. A* **2003**, *107*, 1574–1583.

(75) Koverga, V.; Juhász, A.; Dudariev, D.; Lebedev, M.; Idrissi, A.; Jedlovszky, P. Local Structure of DMF–Water Mixtures, as Seen from Computer Simulations and Voronoi Analysis. *J. Phys. Chem. B* **2022**, *126*, 6964–6978.

(76) Scherzinger, C.; Schwarz, A.; Bardow, A.; Leonhard, K.; Richtering, W. Cononsolvency of poly-N-isopropyl acrylamide (PNIPAM): Microgels versus linear chains and macrogels. *Curr. Opin. Colloid Interface Sci.* **2014**, *19*, 84–94.

(77) Liao, W.; Zhang, Y.; Guan, Y.; Zhu, X. X. Gelation Kinetics of Thermosensitive PNIPAM Microgel Dispersions. *Macromolec. Chem. Phys.* **2011**, *212*, 2052–2060.

(78) Lodge, T. P.; Heimenz, P. C. *Polymer Chemistry*, 3rd ed.; CRC Press: Boca Raton, FL, 2020.

(79) Soetrisno, D. D.; Martínez Narváez, C. D. V.; Sharma, V.; Conrad, J. C. Concentration Regimes for Extensional Relaxation Times of Unentangled Polymer Solutions. *Macromolecules* **2023**, *56*, 4919–4928.

(80) Anna, S. L.; McKinley, G. H.; Nguyen, D. A.; Sridhar, T.; Muller, S. J.; Huang, J.; James, D. F. An interlaboratory comparison of measurements from filament-stretching rheometers using common test fluids. *J. Rheol.* **2001**, *45*, 83–114.

(81) Burchard, W. In *Branched Polymers II*; Roovers, J., Ed.; Advances in Polymer Science; Springer: Berlin, Heidelberg, 1999; Vol. 143; pp 113–194.

(82) Brézault, A.; Perrin, P.; Sanson, N. Multiresponsive Supramolecular Poly(*N* -isopropylacrylamide) Microgels. *Macromolecules* **2024**, *57*, 2651–2660.

(83) Varga, I.; Gilányi, T.; Mészáros, R.; Filipcsei, G.; Zrínyi, M. Effect of Cross-Link Density on the Internal Structure of Poly(*N* -isopropylacrylamide) Microgels. *J. Phys. Chem. B* **2001**, *105*, 9071–9076.

(84) Clara-Rahola, J.; Fernandez-Nieves, A.; Sierra-Martin, B.; South, A. B.; Lyon, L. A.; Kohlbrecher, J.; Fernandez Barbero, A. Structural properties of thermoresponsive poly(N-isopropylacrylamide)-poly(ethyleneglycol) microgels. *J. Chem. Phys.* **2012**, *136*, 214903.

(85) Seery, T. A. P.; Yassini, M.; Hogen-Esch, T. E.; Amis, E. J. Static and dynamic light scattering characterization of solutions of hydrophobically associating fluorocarbon-containing polymers. *Macromolecules* **1992**, *25*, 4784–4791.

(86) Martínez Narváez, C. D. V.; Dinic, J.; Lu, X.; Wang, C.; Rock, R.; Sun, H.; Sharma, V. Rheology and Pinching Dynamics of Associative Polysaccharide Solutions. *Macromolecules* **2021**, *54*, 6372–6388.

(87) Tan, H.; Tam, K.; Tirtaatmadja, V.; Jenkins, R.; Bassett, D. Extensional properties of model hydrophobically modified alkali-soluble associative (HASE) polymer solutions. *J. Nonnewton. Fluid Mech.* **2000**, *92*, 167–185.

(88) Lhota, R. C.; Learsch, R. W.; Temme, J.; Coburn, V.; Kornfield, J. A. Mist-control

of polyalphaolefin (PAO) lubricants using long pairwise end-associative polymers. *J. Nonnewton. Fluid Mech.* **2024**, *326*, 105197.

(89) Tirtaatmadja, V.; McKinley, G. H.; Cooper-White, J. J. Drop formation and breakup of low viscosity elastic fluids: Effects of molecular weight and concentration. *Phys. Fluids* **2006**, *18*, 043101.

(90) Clasen, C.; Plog, J. P.; Kulicke, W.-M.; Owens, M.; Macosko, C.; Scriven, L. E.; Verani, M.; McKinley, G. H. How dilute are dilute solutions in extensional flows? *J. Rheol.* **2006**, *50*, 849–881.

(91) Moelbert, S.; De Los Rios, P. Hydrophobic Interaction Model for Upper and Lower Critical Solution Temperatures. *Macromolecules* **2003**, *36*, 5845–5853.

(92) Paschek, D. Heat capacity effects associated with the hydrophobic hydration and interaction of simple solutes: A detailed structural and energetical analysis based on molecular dynamics simulations. *J. Chem. Phys.* **2004**, *120*, 10605–10617.

(93) Silverstein, K. A. T.; Haymet, A. D. J.; Dill, K. A. The Strength of Hydrogen Bonds in Liquid Water and Around Nonpolar Solutes. *J. Am. Chem. Soc.* **2000**, *122*, 8037–8041.

TOC Graphic